# Gemini South Adaptive Optics Imager (GSAOI)

Peter McGregor[a], John Hart[a], Dejan Stevanovic[a], Gabe Bloxham[a], Damien Jones[b], Jan van Harmelen[a], Jason Griesbach[a], Murray Dawson[a], Peter Young[a], and Mark Jarnyk[a]
[a]Research School of Astronomy and Astrophysics, The Australian National University, Cotter Road, Weston, ACT Australia 2611;
[b]Prime Optics, 17 Crescent Rd., Eumundi, Queensland Australia, 4562

## ABSTRACT

The Gemini South Adaptive Optics Imager (GSAOI) is the science camera and commissioning instrument for the Multi-Conjugate Adaptive Optics (MCAO) system on the Gemini South telescope. GSAOI is required to deliver diffraction-limited performance at near-infrared wavelengths over a 85″×85″ field of view. It must be delivered on a short timescale commensurate with MCAO delivery. GSAOI will use a high throughput, all-refractive optical design and a mosaic of four HAWAII-2RG detectors to form an imager focal plane of 4080x4080 pixels with a fixed scale of 0.02″/pixel. The On-Detector Guide Window (ODGW) capability of the HAWAII-2RG detectors will be used for flexure monitoring and as near-infrared substitutes for MCAO natural guide star wave front sensors. The imager will include a pupil viewer for accurate alignment to MCAO and defocus lenses to measure wave front phase errors at the science detector using the curvature technique. Non-common path wave front errors will be nulled by setting the base shapes of the three MCAO deformable mirrors. The science drivers, performance predictions, optical design issues, and detector system for the instrument are described.

**Keywords:** near-infrared, instrumentation, imager, Gemini, optical design, detector system

## 1. INTRODUCTION

The Gemini 8-m telescopes are designed to achieve unprecedented ground-based image quality using adaptive optics (AO) techniques. This has been demonstrated with Hokupa'a on Gemini North, and with ALTAIR. These are classical AO systems that are restricted in their corrected fields and sky coverage. The Gemini South Multi-Conjugate Adaptive Optics (MCAO) system is being designed to overcome these limitations. MCAO will provide uniform, diffraction-limited image quality at near-infrared wavelengths across an extended field-of-view. Useful levels of atmospheric seeing correction will be achieved over a two arcminute diameter field-of-view, the maximum possible with the Gemini telescope design. Sky coverage will also be comparable to the ALTAIR laser guide star (LGS) system, or somewhat superior to it. MCAO will use three deformable mirrors conjugated to distinct altitude ranges in the atmosphere. These will be driven with commands computed from wave front sensor measurements of five LGSs and three natural guide stars (NGSs). Mean zenith Strehl ratios of 0.2 at *J*, 0.4 at *H*, and 0.6 at *K* will be achieved in median seeing on Cerro Pachon over a one arcminute diameter field using bright NGSs. These will decline to 0.05 at *J*, 0.18 at *H*, and 0.39 at *K* at a zenith distance of 45º. The MCAO system will be able to operate with fewer than three NGSs but with reduced performance.

The Gemini South Adaptive Optics Imager (GSAOI) will be the workhorse instrument used with MCAO. GSAOI is a near-infrared, diffraction-limited, imaging system. GSAOI has a single fixed-format camera with 0.02″ pixels that Nyquist sample the 0.042″ FWHM diffraction-limited images produced at 1.65 $\mu$m, but slightly under-samples the 0.032″ FWHM images at *J*, and slightly over-samples the 0.057″ FWHM images at *K*. GSAOI uses a mosaic of Rockwell HAWAII-2RG HgCdTe/CdZnTe Molecular Beam Epitaxy (MBE) detectors with 4080×4080 18 $\mu$m pixels arranged in four 2040×2040 quadrants each separated by 2.5 mm. Thus GSAOI records a square field-of-view 84.7″ on a side. This neatly fits within the 120″ circular field delivered by the MCAO system. The GSAOI optics have stable and low distortion that will permit high precision astrometric observations, which will be limited in performance only by the stability of MCAO. A comprehensive suite of broad-band and narrow-band filters will be available. GSAOI will combine high throughput with excellent and uniform image quality to provide a high sensitivity MCAO imaging system.

Ground-based Instrumentation for Astronomy, edited by
Alan F. M. Moorwood, Masanori Iye, Proceedings of SPIE Vol. 5492
(SPIE, Bellingham, WA, 2004) · 0277-786X/04/$15 · doi: 10.1117/12.550288

GSAOI must be ready for commissioning MCAO subsystems in early 2006. Consequently, a major design driver has been the reuse of many existing instrument designs in order to commission GSAOI on Gemini South ahead of MCAO availability. This has necessitated reusing the Near-Infrared Imager (NIRI) cryostat design, integration frame design, mechanism encoding system, temperature control system, and Instrument Sequencer and Components Controller software. The Australian National University (ANU) pioneered this approach with great success in fast-tracking the design and construction of NIFS[1].

## 2. SCIENCE DRIVERS

The key science drivers for GSAOI were identified at a Gemini community workshop at Santa Cruz in October 2000 where the main science drivers for MCAO imaging were articulated. GSAOI will address the following diverse science that extends from studies of nearby low mass stars to studies of distant forming galaxies:

- Low mass stellar and substellar mass functions in young star-forming regions such as the Orion Nebula Cluster.
- Stellar population variations in star-forming regions such as Ophiuchus, Corona Australis, and Chamaeleon.
- Open cluster mass functions to the bottom of the H-burning sequence and the end of the white dwarf cooling sequence to provide independent age determinations.
- Mass functions in nearby globular clusters over a range of metallicities.
- Stellar populations of super-star cluster analogs in the Galaxy and Magellanic Clouds such as NGC 3603 and 30 Doradus.
- Missing mass in Magellanic Cloud planetary nebulae.
- Proper motions of Local Group galaxies.
- Stellar populations in dwarf galaxies.
- Stellar populations in starburst regions of nearby galaxies.
- Evolution of dwarf irregular versus elliptical galaxies in different environments.
- Early chemical histories of nearby galaxy spheroids.
- Color distributions among extragalactic globular clusters.
- Measuring $H_0$ out to 60 Mpc using red supergiants.
- Measuring the bulk motion of galaxies to $cz < 6000$ km s$^{-1}$ with surface brightness fluctuations.
- Spatially resolved spectral energy distributions of high redshift field galaxies.
- Evolution of galaxies in clusters.
- The formation of the disks of disk galaxies.
- Exploring dark energy via high redshift supernovae.

A common characteristic of these programs is that they require extremely deep near-infrared photometric imaging of extended regions. This necessitates high system throughput, excellent image quality, and a uniform PSF over the available field. Many science programs encompass large samples of objects that can be selected to have suitable MCAO natural guide stars.

## 3. INSTRUMENT DESCRIPTION

The GSAOI imager forms the science path of the instrument. The 2 arcminute diameter f/34 MCAO output field is directed to GSAOI by the science fold mirror in the Instrument Support Structure (ISS) of the Gemini telescope. The beam passes through the GSAOI cryostat window and the central 85″×85″ square science field comes to focus 300 mm inside the cryostat at a field mask. The beam then passes through a doublet field lens and a four-element optical relay. The field lens forms a pupil image within the relay optics where the internal cold stop is located. Two filter wheels are located immediately in front of this cold stop. The relay reimages the focal plane onto the imager detector at a scale of 0.02″/pixel. A utility wheel allows a pupil viewer lens group to be positioned temporarily between the relay and the detector to record an image of the cold stop. This cold stop image will be used to accurately align the cryostat with the MCAO exit pupil. Convex and concave lenses, also in the utility wheel, produce defocused star images at the detector. These images will be used to measure static wave front phase errors that will be nulled using the MCAO deformable mirrors.

### 3.1. Filter Suite

The contents of the GSAOI filter wheels are listed in Table 1 and Table 2. These contain standard near-infrared broad-band filters and zero-redshift near-infrared emission- and absorption-line filters.

**Table 1: Upper Filter Wheel Contents**

| Position | Filter | $\lambda_c$ ($\mu$m) | $\Delta\lambda$ ($\mu$m) | 50% cut on | 50% cut off |
|---|---|---|---|---|---|
| 1 | Clear | ... | ... | ... | ... |
| 2 | *Z* | 1.015 | 0.170 | 0.930 | 1.100 |
| 3 | *J* | 1.250 | 0.160 | 1.170 | 1.330 |
| 4 | *H* | 1.635 | 0.290 | 1.490 | 1.780 |
| 5 | *K'* | 2.120 | 0.340 | 1.950 | 2.290 |
| 6 | *Ks* | 2.150 | 0.320 | 1.990 | 2.310 |
| 7 | *K* | 2.200 | 0.340 | 2.030 | 2.370 |
| 8 | *J* continuum | 1.207 | 0.018 | 1.198 | 1.216 |
| 9 | *H* continuum | 1.570 | 0.024 | 1.558 | 1.582 |
| 10 | $CH_4$ (short) | 1.580 | 0.100 | 1.530 | 1.630 |
| 11 | $CH_4$ (long) | 1.690 | 0.100 | 1.640 | 1.740 |
| 12 | *Ks* continuum | 2.093 | 0.031 | 2.078 | 2.108 |
| 13 | *Kl* continuum | 2.270 | 0.034 | 2.253 | 2.287 |
| 14 | Spare | ... | ... | ... | ... |
| 15 | Spare | ... | ... | ... | ... |

**Table 2: Lower Filter Wheel Contents**

| Position | Filter | $\lambda_c$ ($\mu$m) | $\Delta\lambda$ ($\mu$m) | 50% cut on | 50% cut off |
|---|---|---|---|---|---|
| 1 | Clear | ... | ... | ... | ... |
| 2 | He I 1.0830 $\mu$m | 1.083 | 0.016 | 1.075 | 1.091 |
| 3 | H I Pγ | 1.094 | 0.011 | 1.089 | 1.100 |
| 4 | H I Pβ | 1.282 | 0.019 | 1.272 | 1.292 |
| 5 | [Fe II] 1.644 $\mu$m | 1.644 | 0.025 | 1.631 | 1.656 |
| 6 | $H_2O$ | 2.000 | 0.080 | 1.960 | 2.040 |
| 7 | He I (2p2s) | 2.058 | 0.031 | 2.042 | 2.073 |
| 8 | $H_2$ 1-0 S(1) | 2.122 | 0.032 | 2.106 | 2.138 |
| 9 | H I Brγ | 2.166 | 0.032 | 2.150 | 2.182 |
| 10 | $H_2$ 2-1 S(1) | 2.248 | 0.034 | 2.231 | 2.265 |
| 11 | CO $\Delta$v=2 | 2.360 | 0.080 | 2.320 | 2.400 |
| 12 | Spare | … | … | … | … |
| 13 | Spare | … | … | … | … |
| 14 | Spare | … | … | … | … |
| 15 | Blocked | … | … | … | … |

### 3.2. Imager Detector

The imager detector is a 4080×4080 pixel mosaic of four three-side buttable 2040×2040 pixel Rockwell HAWAII-2RG HgCdTe/CdZnTe MBE devices with 18 $\mu$m pixels. The four detectors are each separated by ~ 2.5 mm. An additional four rows and columns around the outer edge of each detector are not illuminated. These are read out as reference pixels. The imager detector mosaic is read out in ~ 10 s through 16 video lines. Fowler sampling and correlated double-

sampling readout methods will be implemented. The minimum integration time is ~ 5 s using the correlated double-sampling readout method.

Each imager detector also has a programmable rectangular On-Detector Guide Window (ODGW) capability. This will be used to either monitor slow tip-tilt variations due to flexure between MCAO and GSAOI directly at the imager detector or to provide rapid NGS tip-tilt information to MCAO. It will frequently be convenient to use the near-infrared images of the MCAO NGSs for the former purpose. Guide windows of either 4×4, 8×8, 12×12, 16×16, or 32×32 pixels can be specified.

### 3.3. Imager Quick Look Displays

It is envisaged that data from the imager detector will be presented in two Quick Look Displays; the View Mode Quick Look Display and the Observe Mode Quick Look Display. Temporary data will be obtained and displayed in View Mode, but will not be archived. Science data will be obtained and displayed in Observe Mode. Observe Mode data will be archived.

### 3.4. Non-Common Path Phase Errors

Imaging performance is improved if the MCAO deformable mirrors can be configured to correct non-common path wave front phase errors introduced by the GSAOI optics. Normally, the MCAO Diagnostic Wave Front Sensor is used to flatten the wave front exiting the MCAO system. It is preferable to ensure that the wave front reaching the imager detector is flat. This will be achieved by recording images on either side of focus and analyzing them in the manner described by Roddier& Roddier[2]. The light source for these images will be the MCAO NGS source simulator. This is a 5×5 grid of fiber-fed sources that will produce separated defocused images. The images will be defocused using the convex and concave defocus lenses in the GSAOI utility wheel.

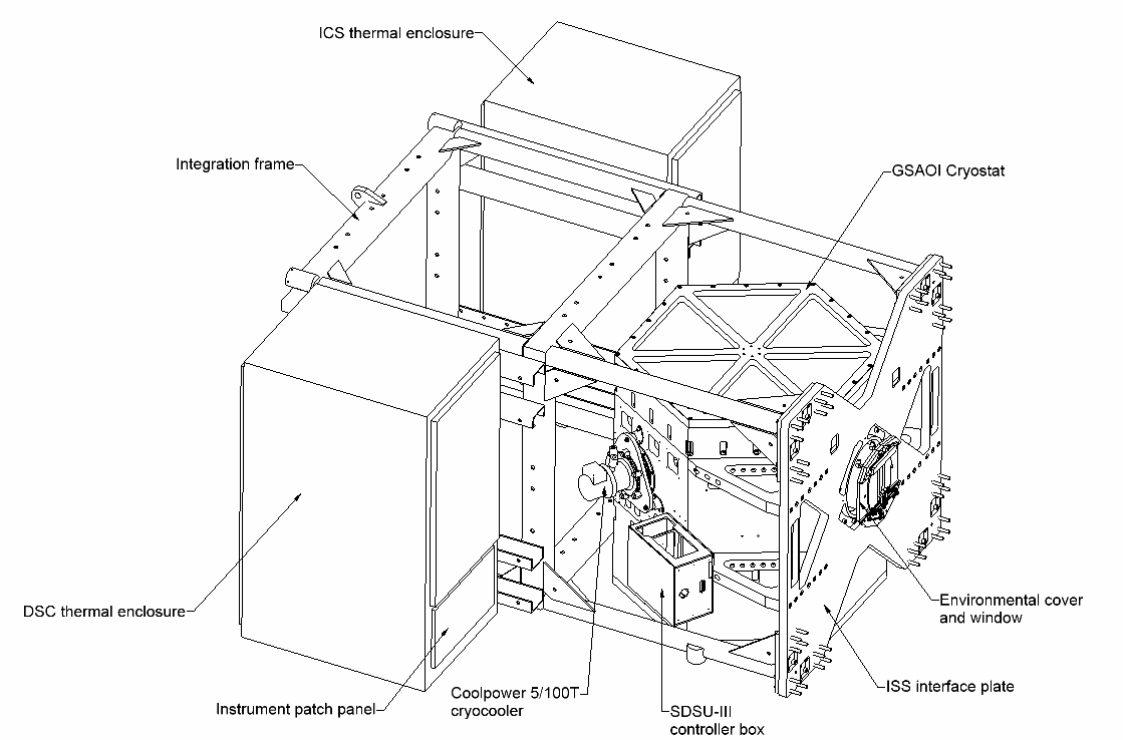


**Figure 1: GSAOI cryostat, ISS interface plate, integration frame, and thermal enclosures.**

### 3.5. Cryostat and Auxiliary Systems

GSAOI is a fast-tracked instrument that is intended to be available for MCAO commissioning. Duplicates of the NIRI/NIFS cryostat, integration frame, instrument control system, and control software will be used to reduce development time.

The cryostat is a hexagonal cylinder 1.0 m in diameter and 1.3 m long (Figure 1). The circular cryostat window has been enlarged to accommodate the 2 arcminute diameter f/34 MCAO field. The exterior of GSAOI is similar to NIRI and NIFS in other ways. An environmental cover is located in front of the cryostat window to protect it and prevent dust accumulation when GSAOI is not in use. The cryostat mounts on the ISS via the ISS interface plate. The SDSU-III controller used to control the GSAOI detector mounts directly on the outside of the cryostat. All other electronics are located in two thermal enclosures.

The two thermal enclosures are carried on the integration frame. One thermal enclosure contains the mechanism and temperature control electronics and the Instrument Control System Input-Output Controller (IOC). The second thermal enclosure contains the SDSU-III power supply and the Detector Control System IOC. The integration frame mounts on the ISS interface plate along with the cryostat but does not load the cryostat.

## 4. INSTRUMENT PERFORMANCE

### 4.1. Imager Sensitivity

Imager sensitivity has been quantified using a model for the object and background signals and assumed detector dark current (0.05 e/s/pix) and read noise (5 e using multiple reads). The model assumes a detector quantum efficiency of ~ 80% (Hall, priv. comm.). Background signals considered are airglow emission and thermal emission from the sky, telescope, MCAO system, cryostat window, and cryostat interior. Limiting magnitudes for a total on-source integration time of 1 hr in 0.4″ seeing through a 0.08″×0.08″ square aperture are listed for each filter in Table 3 along with the Strehl ratio that was assumed for that filter and the sky brightness that resulted.

Saturation magnitudes for each filter are also listed in Table 3. These are calculated for an assumed minimum integration time of 5 s and a detector full well depth of 50,000 e. The same 0.4″ seeing and Strehl ratios listed in Table 3 apply. The faint broad-band saturation magnitudes present a calibration problem: faint near-infrared photometric standards[3] typically have $K$ ~ 10-12 mag. It will be necessary to read out only a sub-region of the imager detector so as not to saturate these standard stars. The brightest standards can be recorded in a 256×256 sub-region (5.1″×5.1″) that is read out 32 times faster than the full array using a minimum integration time of 0.16 s (because only two detector outputs can be used instead of four).

Modeled background signals for each filter have also been calculated. Airglow line emission dominates for all broad-band filters and most narrow-band filters. Thermal emission from the MCAO system makes a major contribution in the three broad $K$ bands and is dominant in the longer wavelength narrow-band filters. These background signals ensure that GSAOI with a read noise of 10 e will be background limited in integration times > 15 s at $Z$, > 4 s at $H$, and > 2 s at $K$, and in integration times > 120 s with all narrow-band filters. Many narrow-band filters will be strongly background limited in this time.

### 4.2. On-Detector Guide Window Sensitivity

The On-Detector Guide Window performance has been estimated using the imager performance model to generate star frames that have then been centroided and the RMS centroiding accuracy determined from 200 simulated guide star frames. Limiting magnitudes that achieve a centroiding accuracy of ~ 2 mas (i.e., 0.1 pix) in integration times of 0.01 s (i.e., when used as a MCAO NGS) and 30 s (i.e., when monitoring flexure variations) are listed for each broad-band filter in Table 4. Also listed are the magnitudes of stars that will just saturate the detector in these integration times.

The availability of faint guide stars at near-infrared wavelengths has been investigated by Spagna[c] for the James Webb Space Telescope. He tabulates cumulative star counts from which probabilities can be calculated that the 2 arcminute diameter MCAO field for any science object will contain at least one guide star brighter than a particular limit. The probability of finding at least one $K \leq 13$ mag guide star, suitable for use as a MCAO NGS with the broad-band filters, in the MCAO field is > 11% while the probability of finding at least one $K \leq 20$ mag guide star, suitable for flexure monitoring with the broad-band filters, in the MCAO field is high (> 97%).

**Table 3: Imager Sensitivities (10:1 in 1 hr)**

| Filter | Limiting Magnitude (mag) | Saturation Magnitude (mag) | Assumed Strehl Ratio | Sky Brightness (mag/arcsec$^2$) |
|---|---|---|---|---|
| *Z* | 25.6 | 14.8 | 0.2 | 17.1 |
| *J* | 24.1 | 13.9 | 0.2 | 14.9 |
| *H* | 24.1 | 14.0 | 0.4 | 14.0 |
| *K'* | 23.9 | 13.3 | 0.6 | 13.5 |
| *Ks* | 23.8 | 13.2 | 0.6 | 13.4 |
| *K* | 23.7 | 13.2 | 0.6 | 13.3 |
| *J* continuum | 23.1 | 11.7 | 0.2 | 15.0 |
| *H* continuum | 22.9 | 11.5 | 0.4 | 14.1 |
| $CH_4$ (short) | 23.6 | 13.1 | 0.4 | 13.9 |
| $CH_4$ (long) | 23.4 | 12.7 | 0.4 | 13.8 |
| *Ks* continuum | 22.7 | 10.9 | 0.6 | 13.6 |
| *Kl* continuum | 22.5 | 10.6 | 0.6 | 13.5 |
| He I 1.0830 $\mu$m | 23.7 | 12.0 | 0.2 | 16.1 |
| H I P$\gamma$ | 23.5 | 11.5 | 0.2 | 16.2 |
| H I P$\beta$ | 22.5 | 11.5 | 0.2 | 14.0 |
| [Fe II] 1.644 $\mu$m | 22.7 | 11.4 | 0.4 | 13.8 |
| $H_2O$ | 23.3 | 11.8 | 0.6 | 13.9 |
| He I (2s2p) | 22.5 | 10.8 | 0.6 | 13.3 |
| $H_2$ 1-0 S(1) | 22.6 | 10.8 | 0.6 | 13.4 |
| H I Br$\gamma$ | 22.6 | 10.7 | 0.6 | 13.5 |
| $H_2$ 2-1 S(1) | 22.5 | 10.6 | 0.6 | 13.5 |
| CO ($\Delta$v=2) | 22.4 | 11.2 | 0.6 | 12.6 |

**Table 4: ODGW Sensitivities (2 mas RMS)**

| Filter | Limiting Magnitude 10 ms integration (mag) | Saturation Magnitude 10 ms integration (mag) | Limiting Magnitude 30 s integration (mag) | Saturation Magnitude 30 s integration (mag) |
|---|---|---|---|---|
| *Z* | 15.1 | 8.0 | 22.7 | 16.7 |
| *J* | 14.2 | 7.1 | 21.2 | 15.8 |
| *H* | 14.5 | 7.3 | 21.0 | 16.0 |
| *K'* | 13.7 | 6.6 | 20.4 | 15.2 |
| *Ks* | 13.6 | 6.5 | 20.3 | 15.2 |
| *K* | 13.5 | 6.5 | 20.2 | 15.1 |

[c] http://www.ngst.nasa.gov/public/unconfigured/doc_0422/rev_03/NGST_GS_report5.pdf

## 5. OPTICAL DESIGN

The basic function of the imager is to re-image the MCAO field onto the detector at a scale of 0.02″/pixel. In the process, it must form an image of the pupil on a cold stop to reject stray radiation. The detector pixels are 18 $\mu$m square and the focal length of the telescope plus MCAO system is 262200 mm. The required magnification of the imager is therefore 0.708. A facility to image the pupil onto the detector for diagnostic purposes is also provided, as is a wave front sensor to facilitate focusing and to allow correction of static aberrations in the whole optical system using MCAO.

### 5.1. Imager

The imager consists of the cryostat window, a field lens, and an optical relay system. Filters are placed in a non-collimated region that is located in front of the cold stop. All filters are required to have the same optical thickness to avoid defocus. The beam onto the detector is non-telecentric. The unfolded optical layout is shown in Figure 2. The total length of the system, from cryostat window to detector, is 1917 mm.

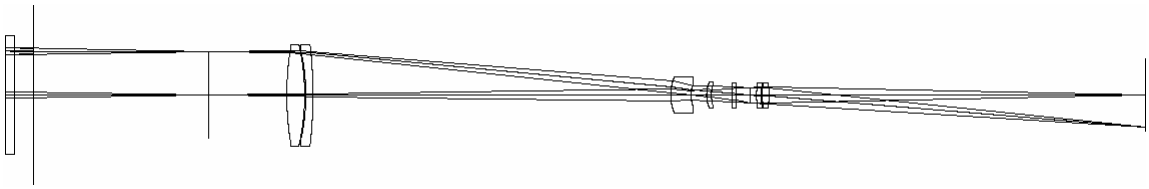

**Figure 2: Unfolded imager optical layout.**

The folding required to fit the layout within the cryostat is shown in Figure 3. Three fold mirrors are employed.

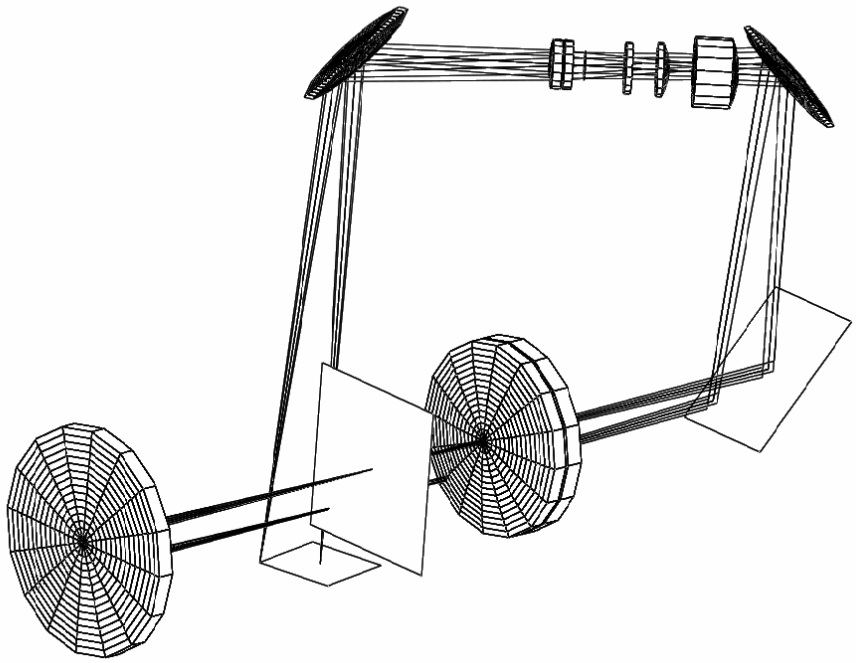

**Figure 3: Folded layout of the imager.**

The cryostat window is Infrasil 302, with a slightly convex outer surface to attenuate the ghost image produced by internal reflection. Following the window is the MCAO focal plane, a doublet field lens of calcium fluoride and Infrasil 302, a thick zinc selenide meniscus, and a barium fluoride singlet lens. The filter, which has a diameter of ~ 26 mm, is placed in the space before the cold stop. Thereafter, a doublet of Infrasil 301 and barium fluoride forms the non-telecentric beam onto the detector. The filters operate in an f/10 beam, so their thickness must be controlled to prevent unacceptable focus displacement and scale change. The required tolerance is ±0.025 mm.

The relay design has excellent image quality as shown in Figure 4. The box size is 2×2 detector pixels (0.04″×0.04″) and all share the same focus position. The field positions are shown for the center, edge, and corner positions of the detector. The wavelengths are for the center of the *Z*, *J*, *H*, and *K* bands. System performance will be dominated by aberrations introduced by the MCAO system. Distortion in the relay design is below 0.005%, which is excellent; the maximum grid displacement is 0.1 pixels. System distortion will also be dominated by asymmetric distortion introduced by the two MCAO off-axis parabolas.

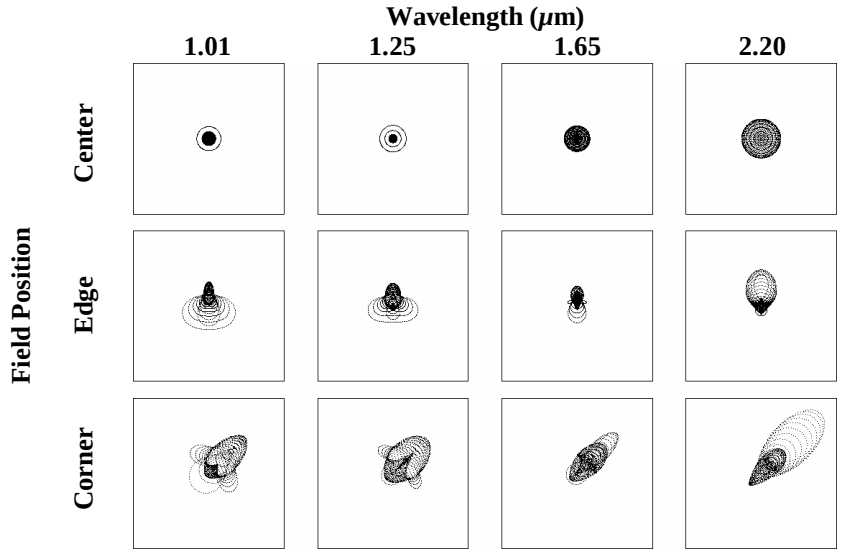


**Figure 4: Spot diagrams for the imager relay design. Boxes are 2 pixels square.**

Figure 5 shows the pupil image tilt caused by the off-axis MCAO optics. The cold stop is tilted by 23° to be coincident with the pupil image, so optimizing its masking performance. The rays are traced from an object plane on the Gemini secondary mirror with the square GSAOI focal plane mask acting as the pupil for the imaging process. The average RMS blurring at the cold stop edge is 0.6% of the cold stop diameter. The axial position of the cold stop has been optimized for the *H* and *K* bands where the cold stop needs to be most effective.

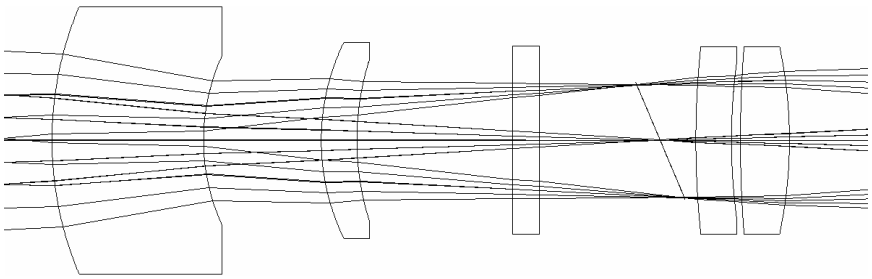

**Figure 5: Tilted cold stop in the MCAO/GSAOI assembly.**

The optical relay has excellent ghost image performance. Features that contribute to this performance are:

- The non-telecentric geometry tends to exclude ghosts involving reflection at the detector.
- The slight curvature on one window face attenuates the ghost caused by reflection within the window.
- Filter placement in a non-collimated beam attenuates the ghost caused by reflection within the filter.
- The central gap in the detector mosaic eliminates most pupil ghosting.

A ghost image caused by reflection in the detector substrate is potentially problematic because the incident beam is not telecentric. The GSAOI HAWAII-2RG detectors use a 0.82 mm thick CdZnTe substrate (Cabelli, priv. comm.) in front of the HgCdTe detector material. The refractive index of this substrate material is uncertain, but is estimated to be ~ 3.29 at a wavelength of 1 $\mu$m and a temperature of 80 K. The incident ray angle is 6.4º at the edge of the imager field so the chief ray passes through the detector substrate at an angle of ~ 1.9º. A single internal reflection then produces a ghost image with a radial displacement of 56 $\mu$m (3.1 pixels) from the primary image. The displacement is proportional to the field eccentricity and reaches 4.4 pixels at the detector corners.

The ghost intensity cannot be estimated accurately, and so has been estimated conservatively as follows. The quantum efficiency of the detector is between 70 and 85%. Perhaps 10% of the light is reflected from the detector layer. The amount returned to the detector at the CdZnTe/vacuum interface is uncertain and depends on the characteristics of the anti-reflection (AR) coating. If there is no AR coating, ~ 28.5% would be internally reflected at the interface. The high quantum efficiency suggests that more like 10% is internally reflected. Of these photons, ~ 80% will be detected in the ghost image. The ghost intensity will then be ~ 0.1×0.1×0.8 = 0.008 of the primary intensity.

This ghost intensity ratio is considerably higher than the specified limit of $10^{-5}$. It is therefore crucial to decide whether or not the ghost is lost within the AO-corrected PSF because of its small displacement. Simulated images (including the ghost) located near the detector edge suggest that the scientific impact of the detector ghost will be small, even on long exposures of bright stars.

Discussions with Rockwell indicate that reflection at the CdZnTe/HgCdTe interface may be more like 1-2%, rather than the 10% assumed above. This is likely to make the ghost undetectable.

### 5.2. Pupil Viewer

The pupil viewer mode is implemented by the insertion of a group of three lenses between the imager optics and the detector via the utility wheel. The imager optics and the detector are not disturbed. The first two pupil viewer lenses are calcium fluoride and the third is Infrasil 302. Figure 6 shows the unfolded system both with and without the pupil viewer lenses inserted. The real cold stop tilt due to MCAO is not shown.

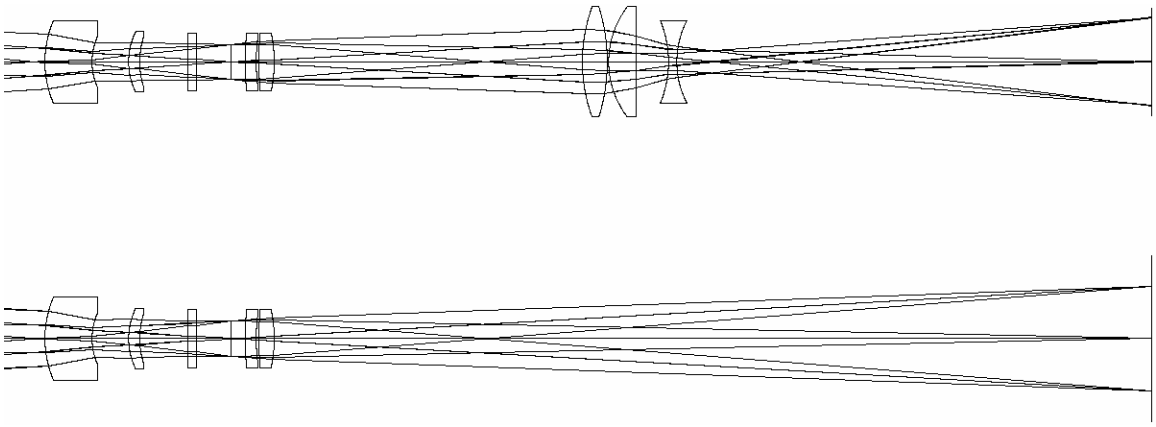

**Figure 6: Layout with (*top*) and without (*bottom*) the pupil viewer.**

### 5.3. Wave Front Sensor

Two sets of lenses will be inserted into the beam at the location of the utility wheel to record defocused images with the focus extended and retracted. The MCAO deformable mirrors will then be adjusted to null non-common-path wave front errors, so correcting static errors in the whole optical system. To maximize sensitivity, the size of the defocused images should be no larger than is required to give adequate resolution. The adopted size of the defocused images is 1.4 mm (78 pixels). The two-pixel resolution then corresponds to 200 mm on the primary mirror, which is adequate in relation to the 500 mm spacing of the MCAO adaptive optics actuators.

Studies of the analysis software have shown that best results are obtained if the two defocused images have the same size, so the lenses have been designed to achieve this. The extender and retractor lenses are mounted in the utility wheel about 375 mm from the detector. Each is a doublet of calcium fluoride and Infrasil 302. The layout of the two defocus lenses is shown in Figure 7.

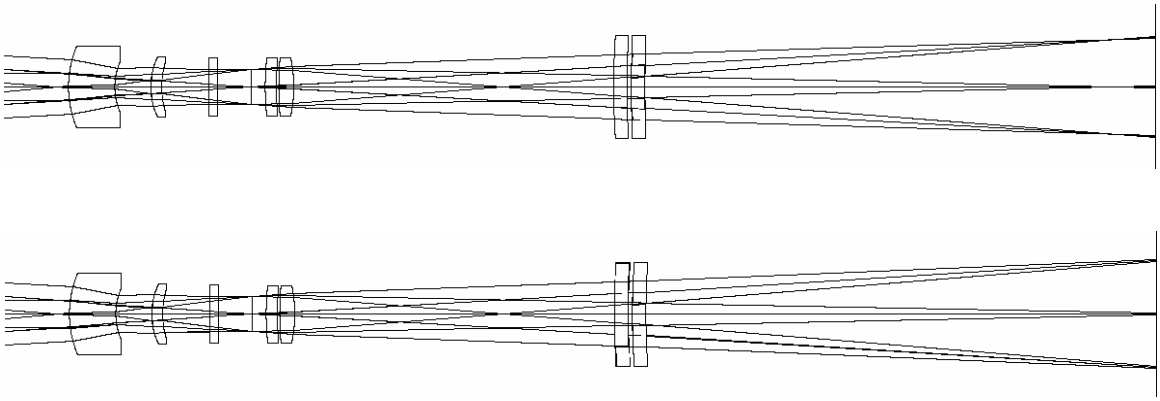

**Figure 7: Layout of lenses for retracted (*top*) and extended (*bottom*) focus positions.**

## 6. DETECTOR CONTROL SYSTEM

The detector control system (DCS) will read out the mosaic of four Rockwell HAWAII-2RG detectors in less than 10 s. Standard noise reduction techniques of correlated double sampling and Fowler sampling will be implemented. On-Detector Guide Windows of arbitrary size and position will be read out during integrations of the full detector mosaic. The focal plane assembly will operate at low temperatures (60-90 K) with a stability of ±1 mK.

### 6.1. Readout Speed

The imager detectors will be read out using the 100 kHz slow readout mode. Three readout speed options will be implemented initially; a fast 300 kHz speed for instrument setup, a medium 200 kHz speed for broad-band observations, and a slow 100 kHz speed for narrow-band observations where low read noise is desirable. Faster read out speeds may be possible with minimal impact on read noise. The correlated double sample full frame read time using the 200 kHz mode and four amplifiers per HAWAII-2RG detector will be ~ 10 s.

### 6.2. Detector Controller

The imager detector controller is based on the Astronomical Research Cameras Inc. Gen. III controller, which is commonly referred to as the SDSU-III. The SDSU-III detector controller housing will be mounted on the vacuum jacket adjacent to the imager detector hermetic connectors. This close proximity to the image detector minimizes wiring capacitance, and so reduces the required drive currents.

The SDSU-III detector controller design consists of the following components:

1. One SDSU-III detector controller configured with the following components:
   - Two modified SDSU Octal Channel IR Video Processor Boards (video boards) configured for H2RG devices. Each board has eight differential video processing channels. The video processing channels have programmable bandwidth and gain.
   - Two custom Bias Boards. Each board provides the 24 ultra low noise, high stability biases and power supplies required for the imager detector mosaic.
   - Two SDSU IR Clock Driver Boards (clock boards). Each board provides 24 clock/bias generators in two banks of 12 clocks/biases. One bank will drive each H2RG detector. The standard clock boards will be modified to provide faster clock rise and fall times.
   - One SDSU 12.5 Mpixel/s Fiber-Optic Timing Board (timing board). This board provides the timing sequencer and the communication hub for the other boards.
   - One SDSU Power Controller, one SDSU 12-slot back plane, and one SDSU enclosed housing.
2. Two fiber-optic communication cables. A 3 m length runs from the timing board to the DCS thermal enclosure input/output connection panel, and a 2 m length runs from the DCS thermal enclosure input/output connection panel to a SDSU PMC interface board.
3. One 12.5 Mpixel/s SDSU PMC interface board. This board plugs into the PMC slot on the Detector Controller IOC processor board. It provides the fiber-optic communication interface between the SDSU-III detector controller and the Detector Controller IOC.
4. An IOC input/output connection panel with two fiber-optic feedthroughs and a power supply feedthrough connector. This panel provides a reliable place to connect and disconnect the fiber-optic cables from the PMC interface board.
5. One air-cooled SDSU-III large power supply for a 12 slot system with custom cables to connect through the IOC input/output connection panel. The power supply is mounted inside the DCS thermal enclosure. A 3 m cable runs from the SDSU-III detector controller to the Detector Controller IOC input/output connection panel, and a 2 m cable runs from the IOC input/output connection panel to the power supply.
6. Custom external wiring manufactured from a composite of cables and wires. This wiring provides the connection from the cryostat hermetic connectors to the SDSU-III detector controller inputs.
7. A custom water jacket and hoses for cooling and temperature stabilizing the SDSU-III detector controller housing.

### 6.3. On-Detector Guide Window

The HAWAII-2RG multiplexer can read out any rectangular region of the pixel array while the remainder of the area is integrating. This feature will be used to implement separate On-Detector Guide Windows (ODGWs) on each of the four imager detectors. These will be read out repeatedly during an imager integration to monitor image translation for tip-tilt or flexure correction.

It is desirable to continue reading the ODGW while a full imager frame is being read out. This would allow fast tip-tilt or slow flexure correction to be initiated before an imager integration commenced and would maintain these functions over the full imager integration time. However, interlacing guide window and imager reads greatly extends the full frame read time at high ODGW frame rates. A compromise solution will be implemented in which the ODGWs are read out at a modest rate during full frame reads and will revert to higher frame rates if required during full frame integrations. The actual frame rates that can be achieved will depend on the performance of the devices.

The H2RG detectors will be configured to read out the ODGW through one of their normal outputs (Output#7). The ODGW data will therefore be processed by the same video channels that process full frame data. The ODGW is sampled at 100 kHz to achieve lower read noise. It is expected that this read noise advantage will be required to detect faint ODGW guide stars with short integration times. A consequence of reading out the ODGW and the full frame at different speeds through the same video channel is that different video bandwidths are required for the different speeds. The programmable bandwidth feature of the video boards will be used to implement this requirement.

## 7. STATUS

GSAOI is being constructed at Mt. Stromlo Observatory in Canberra, Australia. The cryostat has undergone thermal testing. The imager housing and mechanisms are due for installation and test in the cryostat in July 2004. Two engineering detectors and one science detector have been delivered. The instrument is scheduled for shipment to Gemini South in October 2005, and will be commissioned with early versions of MCAO around the beginning of 2006.

## REFERENCES


1. P. McGregor, J. Hart, P. Conroy, L. Pfitzner, G. Bloxham, D. Jones, M. Downing, M. Dawson, P. Young, M. Jarnyk, and J. van Harmelen, "Gemini near-infrared integral field spectrograph (NIFS)", Proc. S.P.I.E., 4841, pp. 1581-1591, 2002.
2. C. Roddier, and F. Roddier, "Wave-front reconstruction from defocused images and the testing of ground-based optical telescopes", JOSA, 10, 2277-2287, 1993.
3. S. E. Persson, D. Murphy, W. Krzeminski, M. Roth, and M. Rieke, "A new system of faint near-infrared standard stars", AJ, 116, pp. 2475-2488, 1998.